Trunk Health Condition Inspection using Integrated 3D Photogrammetry and Holographic Radar Tomography

Lilong Zou, *Senior Member, IEEE,* Xuan Feng, *Senior Member, IEEE,* Hai, Liu, *Senior Member, IEEE,* Amir M. Alani and Cai Liu

***Abstract*—Forests are vital components of the ecosystem of Earth, regulating climate, conserving soil and water, and fostering biodiversity. Sustainable forest management offers crucial long-term benefits, but challenges such as disease threaten tree health. Disease-infected trees, in both forests and urban areas, pose risks to safety, property and culture, leading to economic losses. Traditional inspection methods such as resistance drilling are invasive and laborious while non-destructive techniques such as Ground Penetrating Radar (GPR) offer promising alternatives. Although GPR shows potential, complexities such as tree structure and electromagnetic properties hinder accurate disease detection. To address these challenges, a new approach integrates structure-from-motion (SfM) photogrammetry with GPR measurement, and a novel holographic radar tomography processing has been proposed in this paper. These methodologies accurately reconstruct tree trunks in 3D, enabling precise GPR positioning and the obtaining of trunk permittivity. Moreover, an arc-shaped Kirchhoff migration algorithm helps mitigate irregular trunk shapes, enhancing data accuracy. The proposed framework demonstrates efficacy in real-tree measurement, offering high-precision disease monitoring. This innovation not only aids in preserving biodiversity but also enhances ecosystem services by promoting sustainable forest management. Effective disease monitoring ensures timely intervention, safeguarding valuable old trees and ecosystems while minimizing economic and cultural losses.**

***Index Terms*—Ground Penetrating Radar (GPR), tree trunk inspection, structure-from-motion (SfM) photogrammetry, Holographic Radar Tomography, Kirchhoff migration, Dual-polarized radar**

I. Introduction

FORESTS are vital to the global ecosystem, playing an essential role in regulating the climate, conserving soil and water, controlling wind and sand, and supporting biodiversity. They provide resources such as timber and raw materials, mitigate natural disasters, purify air, and reduce noise, ensuring environmental stability. As such, it is vital to protect existing forests, and ensure their regeneration, which takes years – around a decade for planted forests and significantly longer for natural forests. Since 1990, over 80 million hectares of primary forest have been lost, with over 100 million hectares damaged by fires, pests, diseases, and extreme weather events [1]-[3]. Protecting forests from pests, diseases, and environmental damage is critical to maintaining ecosystem balance. Urban forests in cities like London and Beijing are also vulnerable, with decaying trees posing risks to public safety and cultural heritage [4][5]. Additionally, comprehensive management of ancient trees, which hold cultural and ecological significance, is essential. Therefore, tree health monitoring is crucial for forest stability, environmental protection, and sustaining the timber industry.

Major factors in the widespread destruction of forests are pests and disease, which typically originate from within tree trunks and can be spread by birds, insects, and vermin. Traditional inspection methods, such as resistance drilling, assess tree decay by detecting reduced resistance in hollow areas. However, this method is invasive and may cause further damage by creating pathways for pathogens [6][7]. Non-destructive testing (NDT) offers a superior alternative for early disease detection while avoiding harm, especially to valuable old trees [8][9]. NDT methods include electrical resistance, nuclear magnetic resonance, X-ray imaging, acoustic tomography, and microwave tomography. Electrical resistance is useful for detecting early decay, but fungal activity can reduce resistivity without actual decay [10]. Magnetic resonance imaging efficiently identifies fungal decay before visual symptoms appear, although its high cost limits its use [11]. X-ray imaging provides a detailed structural analysis but poses radiation risks [12]. Acoustic tomography evaluates decay by measuring wave speed changes, but significant effort must be expended in the deployment of equipment. Microwave tomography detects decay by analyzing attenuation but can be challenging, due to the attendant requirement to deploy multiple

Manuscript received xx xx, xxxx; revised xx xx, xxxx; accepted xx xx, xxxx. Date of publication xx xx, xxxx; date of current version xx xx, xxxx. *(Corresponding author: Lilong Zou.)*

Lilong Zou and Amir M. Alani are with the Faculty of Engineering, Computing and the Environment, Kingston University, London KT1 1LQ, U.K. (e-mail: l.zou@kingston.ac.uk; m.alani@kingston.ac.uk).

Xuan Feng and Cai Liu are with the College of Geo-Exploration Science and Technology, Jilin University, Changchun 130026, Jilin, China (e-mail: fengxuan@jlu.edu.cn; liucai@jlu.edu.cn).

Hai Liu is with the School of Civil Engineering, Guangzhou University, Guangzhou 510006, China (e-mail: hliu@gzhu.edu.cn).

transmitters and receivers around cross-sections, requiring time and effort. Despite their limitations, these NDT methods are crucial for preserving forests and ensuring their ecological and cultural sustainability [13]-[15].

Ground Penetrating Radar (GPR) is a reliable NDT method widely applied in geotechnical engineering, archaeology, and civil engineering. It has significant potential in estimating root parameters [16]-[18] and assessing trunk health [19]-[21] by detecting decay and interlayer interfaces through reflected and diffracted signals. While GPR is effective for identifying large internal areas of damage or cavities in tree trunks, research on early decay detection and small cavities remains limited. The complexity of living tree structures and their electromagnetic properties complicates GPR signal interpretation. Tree trunks consist of multiple layers, including the cork layer (bark), cork-forming layer, green bark, vascular bundles, wood (sapwood and heartwood), and pith. Bark allows the high penetration of electromagnetic waves but produce diffuse reflections due to its rough surface. The cork-forming layer, rich in minerals and solutes, acts as a conductive medium, blocking most waves and leaving minimal signals for analysis. Additionally, irregular trunk shapes and complex reflection curves challenge precise tracing and image processing. Traditional algorithms struggle with these complexities, particularly with small-scale targets such as tree trunks, making data interpretation difficult [8][22].

Therefore, to overcome these challenges, this paper introduces an innovative method for monitoring and detecting tree disease, advancing biodiversity conservation and providing ecosystem services. The approach integrates several novel technologies to overcome traditional challenges in tree health monitoring. Central to this strategy is the combination of Structure-from-Motion (SfM) photogrammetry and GPR surveying. SfM enables a precise reconstruction of the three-dimensional (3D) structure of tree trunks, allowing an accurate interpolation of GPR operating tracks in the 3D space. This enhances the effectiveness and accuracy of GPR in detecting subsurface targets.

Meanwhile, a novel holographic radar tomography process by which to determine the 3D relative permittivity of tree trunks - a critical parameter for analyzing subsurface materials is also proposed in this paper. While traditional methods, such as hyperbola fitting and common midpoint (CMP) surveys, have been used to estimate relative permittivity, this study enhances these techniques by integrating dual-polarization reflections. Borrowing from techniques used in Martian surface studies [23], this dual-polarization approach improves estimation accuracy and aligns results more closely with real-world conditions. By fusing horizontal-horizontal (HH) and vertical-vertical (VV) reflections, the method boosts the signal-to-noise ratio (SNR), further refining data precision. Furthermore, this paper employes an arc-shaped Kirchhoff migration algorithm which can effectively minimize distortions caused by trunk shapes to address challenges posed by the irregular geometry of tree trunks. These novel combinational approaches represent a significant advancement in tree health monitoring, offering enhanced accuracy and efficiency in diagnosing and mitigating tree diseases while supporting environmental preservation efforts.

The proposed data processing framework has been validated with real-world measurements, demonstrating its effectiveness in monitoring tree health. Results show that this approach successfully detects early decay and minor cavities, enabling timely intervention to prevent further damage. The absence of closed anomalies suggests no severe hollow areas, indicating maintained structural integrity. This innovative methodology offers a precise and efficient strategy for monitoring tree diseases, benefiting forest and urban tree management. Additionally, it supports biodiversity conservation and ecosystem sustainability, providing significant value in terms of both preserving tree health and ensuring the longevity of natural and urban environments.

This article is structured as follows: Section II details the proposed processing strategy, including SfM photogrammetry, holographic radar tomography, and arc-shaped Kirchhoff migration techniques. Section III outlines the real data processing procedure, covering preprocessing, antenna coupling removal, holographic radar tomography, and arc-shaped Kirchhoff migration. Additionally, it discusses the dual-polarized GPR system, tree trunk survey, and SfM technology for recovering GPR traces. Section IV presents results and discussions, while Section V concludes the article.

II. METHODOLOGY

A. SfM Photogrammetry Technique

To solve the challenge caused by the irregular shape of tree trunks, the SfM photogrammetry technique is performed in this paper to extract an accurate survey position of each GPR trace. The basic principle of SfM is similar to the way many modern cameras allow the creation of a panorama by stitching together overlapping photographs into a 2D mosaic. The goal is to find the optimal set of camera parameters and 3D coordinates, to minimize reprojection errors across all images and feature points, while enforcing additional constraints of the estimated 3D structure (as described in Fig. 1(a)). SfM uses the position of the camera as it moves through 3D space to estimate the X, Y and Z coordinates for each pixel of the original image and creates 3D models of the trunk under survey. The SfM problem is a non-linear and non-convex optimization problem that can be solved using iterative optimization techniques [24]-[26].

Let $P_{m,n} = (U_{m,n}, V_{m,n})$ be the 2D coordinates of the n feature points in the m image, and $Q_n = (X_n, Y_n, Z_n)$ be its corresponding 3D coordinates in the world coordinate system. Let K_m be the intrinsic camera matrix of the m camera, and R_m and T_m be its rotation matrix and translation vector, respectively. Then, the projection equation that relates a 3D point Q_n to its image coordinates $P_{m,n}$ is:

$$s_{m,n} * \left[U_{m,n}, V_{m,n}, 1\right]^T = K_m * [R_n|T_m] * [Q_n, 1]^T \quad (1)$$

where $s_{m,n}$ is a scale factor that accounts for the unknown depth of point Q_n.

The SfM problem can be formulated as follows: Given a set of N images and their corresponding 2D feature points (as described in Fig. 1(b)), find the camera parameters K_m, R_m and

T_m, as well as the 3D coordinates Q_n that minimize the reprojection error E, defined as the distance between the observed and predicted image coordinates:

$$E_{m,n} = min\left\|P_{m,n} - K_m * [R_n|T_m] * [Q_n, 1]^T\right\|. \quad (2)$$

Figure 2 shows a processing flow chart that builds a 3D digital elevation model (DEM) of the tree trunk and extracts a GPR survey trace. The features of each input photograph are extracted, and then their spatial coordinates are generated through photograph pairs. Subsequently, a 3D point cloud model is reconstructed by gathering the point cloud data of all photographs. The dense point cloud can be obtained by extending the sparse point cloud between adjacent pixels using a dense matching technique. Finally, a filtering algorithm is used to eliminate the noisy points existing around the target model.

In this paper, we used a single camera capturing image to build a 3D DEM model of surveyed tree trunk. Single-camera SfM accuracy relies heavily on sufficient camera motion, effective feature detection, and handling scale ambiguity and estimation challenges. Robust features matching across images is essential, but environmental factors like lighting and occlusions can lead to inconsistent detection, decreasing accuracy [27]. Additionally, single-camera SfM suffers from scale ambiguity since true scene dimensions are not directly measurable without external data like GPS or known landmarks [28]. Depth estimation also worsens with increased object distance, as the single-camera perspective lacks parallax information critical for precise depth at long ranges, often resulting in inconsistencies in outdoor scenes or with repetitive structures [29]. However, using a single camera reduces equipment costs compared to multi-camera setups and advanced 3D scanning technologies. Moreover, the single-camera setup is lightweight and easy to transport, making it suitable for fieldwork. SfM can achieve sub-centimeter spatial accuracy in close-range or controlled environments, offering spatial precision far exceeding the resolution of the GPR system. This exceptional precision allows the precise alignment of each GPR trace with the surface structure, greatly improving the accuracy of subsurface imaging. The innovative use of photogrammetric techniques to create a detailed 3D model provides valuable context for interpreting GPR survey results, elevating the overall effectiveness of the study in capturing the intricate details of the inner characteristics.

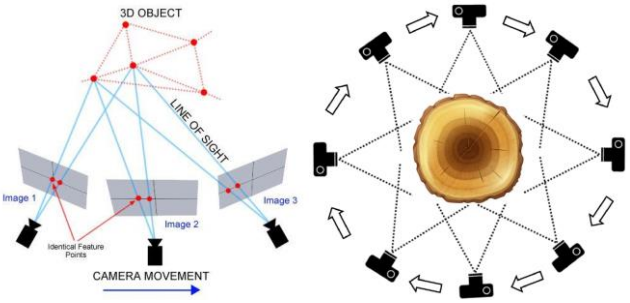

Fig. 1. 3D geometric reconstruction of tree trunk using SfM technique.

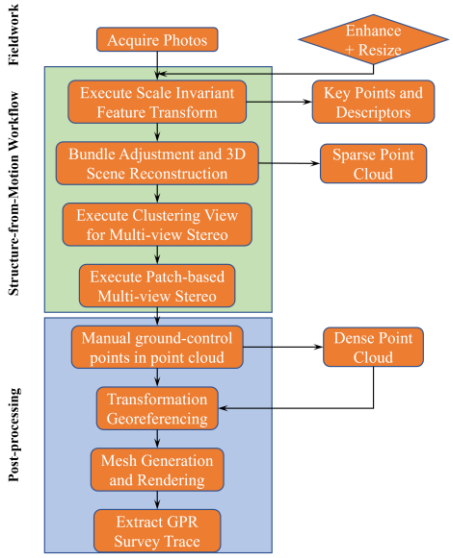

Fig. 2. Flow chart building 3D DEM of tree trunk and extracting GPR survey trace.

B. *Holographic Radar Tomography*

As shown in Fig. 3, EM waves propagate through the GPR transmitter antenna and transmit incident field into the tree trunk. Relying on Maxwell equations, the scattered field is formed by means of complex, frequency-dependent global reflection and transmission coefficients of observation medium [30][31]. These characteristic coefficients are determined by the antenna and reflections, and thereby the scattered fields [32]. When the same antenna is simultaneously used as the transmitter and receiver for the HH and VV modes, the relationship between the radar-measured fields of HH and VV are described in the frequency domain as follows:

$$S_{HH}(\omega) = \frac{B_{HH}(\omega)}{A_{HH}(\omega)} = R_{HH}(\omega) + T^i_{HH}(\omega)\mathcal{F}_{HH}(\omega)T^s_{HH} \quad (3)$$

$$S_{VV}(\omega) = \frac{B_{VV}(\omega)}{A_{VV}(\omega)} = R_{VV}(\omega) + T^i_{VV}(\omega)\mathcal{F}_{VV}(\omega)T^s_{VV} \quad (4)$$

where $S_{HH}(\omega)$ and $S_{VV}(\omega)$ are the HH and VV reflected signals, respectively. The reflected signals can be expressed as the ratio between the backscattered field $B(\omega)$ and incident field $A(\omega)$ at the GPR reference plane. ω indicates the angular frequency. $R_{HH}(\omega)$ and $R_{VV}(\omega)$ are the global reflection for fields from the radar transmitter to receiver, corresponding to the direct antenna coupling of the HH and VV modes, respectively. T^i indicates the transmitter antenna coefficient for incident fields from the radar reference plane onto the target, and T^s indicates the receiver antenna coefficient for fields reflected from the target onto the radar reference plane. $\mathcal{F}(\omega)$

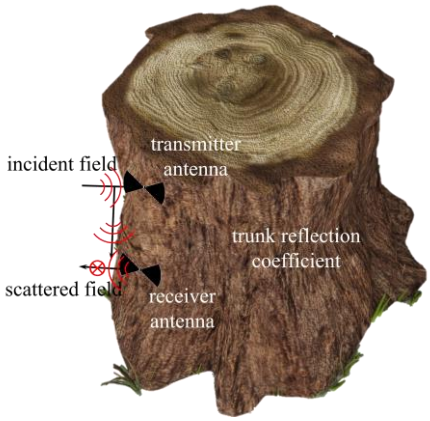

Fig. 3. Illustration of EM wave propagating into tree trunk during GPR survey.

indicates the scattering coefficient of the target and can be expressed as follows:

$$\mathcal{F}_{HH}(\omega) = \mathcal{L}_{HH}(\omega)\varepsilon_{target} \quad (5)$$

$$\mathcal{F}_{VV}(\omega) = \mathcal{L}_{VV}(\omega)\varepsilon_{target} \quad (6)$$

where $\mathcal{L}$ indicates the scattering loss factor and ε_{target} is the global relativity permittivity of the target. The scattering loss factor $\mathcal{L}(\omega)$ can be further detailed as it depends on various physical parameters, including the size, shape, and material properties of the target. It can be expressed as:

$$\mathcal{L}(\omega) = f(\sigma, \lambda, \varepsilon_{target}) \quad (7)$$

where σ is the conductivity of the target. λ is the wavelength of the incident wave.

Since the direct antenna coupling is a static value and can be removed by subtracting the free space radar measurement, Eqs. (3) and (4) can be rewritten as:

$$S'_{HH}(\omega) = T^i_{HH}(\omega)\mathcal{F}_{HH}(\omega)T^s_{HH} \quad (8)$$

$$S'_{VV}(\omega) = T^i_{VV}(\omega)\mathcal{F}_{VV}(\omega)T^s_{VV} \quad (9)$$

Let us assume that $T^i_{HH}(\omega) = T^s_{HH}(\omega) = T^i_{VV}(\omega) = T^s_{VV}(\omega) = T(\omega)$. This means that the antenna coefficients factors of the HH and VV modes are considered to have some value. Therefore, we can have:

$$S'_{HH}(\omega) + S'_{VV}(\omega) = T^2(\omega)\mathcal{L}_{HH}(\omega)\left[1 + \frac{\mathcal{L}_{VV}(\omega)}{\mathcal{L}_{HH}(\omega)}\right]\varepsilon_{target} \quad (10)$$

$$S'_{HH}(\omega) - S'_{VV}(\omega) = T^2(\omega)\mathcal{L}_{HH}(\omega)\left[1 - \frac{\mathcal{L}_{VV}(\omega)}{\mathcal{L}_{HH}(\omega)}\right]\varepsilon_{target} \quad (11)$$

Now, we can give the proposed holographic radar tomography as:

$$\frac{S'_{HH}(\omega)+S'_{VV}(\omega)}{1+\frac{S'_{VV}(\omega)}{S'_{HH}(\omega)}} + \frac{S'_{HH}(\omega)-S'_{VV}(\omega)}{1-\frac{S'_{VV}(\omega)}{S'_{HH}(\omega)}} = \Gamma(\omega)\varepsilon_{target} \quad (12)$$

where $\Gamma(\omega) = 2T^2(\omega)\mathcal{L}_{HH}(\omega)$ is a scaling factor containing scattering loss $\mathcal{L}_{HH}(\omega)$ and antenna coefficient T. After this processing, the GPR profile will be transferred to the target relativity permittivity ε_{target} multiple with a scaling factor of $\Gamma(\omega)$.

C. Arc-shape Kirchhoff Migration

In the pursuit of reconstructing the intricate 3D inner structure of a tree trunk through non-invasive methods, a sophisticated 3D migration algorithm takes center stage. This algorithm is known as 3D Kirchhoff migration. The primary aim of this migration process is to surmount the challenges posed by accurately relocating subsurface targets and their temporal positions to their true subsurface coordinates [33][34]. Compared to traditional methods, a more geometrically precise representation of the internal composition of the tree trunk is offered by 3D Kirchhoff migration. This migration procedure, while effective, can be resource-intensive in terms of both time and cost, particularly when striving for high-resolution outputs. The computational demands and the need for sophisticated equipment contribute to the overall complexity and expense associated with achieving detailed and accurate 3D reconstructions of the inner structure of tree trunks using this method.

In the context of this research paper, a novel arc-shape Kirchhoff migration approach is introduced, incorporating an optimal imaging aperture. The critical selection of the imaging aperture is determined by considering both its equivalent

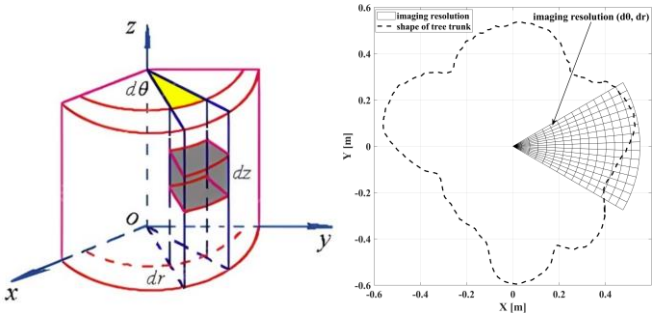

(a) (b)

Fig. 4. Illustration of arc-shape Kirchhoff migration setup: (a) cylindrical coordinate system; (b) arc imaging cell.

diameter and the radiation pattern of the GPR system antenna, as elucidated in Eq. (13). Figure 4 provides a visual representation of the imaging resolution, highlighting its components: an azimuth angle $d\theta$, a radial resolution dr and a vertical resolution dz. Mathematically, the output wave field $F(z_{out}, \theta_{out}, r, t)$ of the tree trunk following Kirchhoff migration is obtained by solving the scalar wave equation from the wave field with zero offset $\Gamma \cdot \varepsilon(z_{in}, \theta_{in}, r_{surface}, t)$, which corresponds to Eq. (10) in the above subsection. The zero offset data is measured at the surface of the tree trunk. The comprehensive migration solution is provided by:

$$F(z_{out}, \theta_{out}, r, t) = \frac{1}{2}\Gamma \iint \left[\frac{cos\alpha}{R^2}\varepsilon\left(z_{in}, \theta_{in}, r_{surface}, t + \frac{R}{v}\right) + \frac{cos\alpha}{vR}\frac{\partial}{\partial t}\varepsilon\left(z_{in}, \theta_{in}, r_{surface}, t + \frac{R}{v}\right)\right] dzdz \quad (13)$$

where v is root mean square (RMS) velocity. R is the path from the target point $(z_{out}, \theta_{out}, r)$ to the observation point $(z_{in}, \theta_{in}, r_{surface})$ at the tree trunk surface. α is the angle of incident wave relating to the antenna radiation pattern.

This strategy for 3D Kirchhoff migration is distinguished by high efficiency, with minimal requirements for computation and operation. In comparison to traditional regular grid-based migration approaches, a finer mesh can be achieved within the trunk by utilizing cylindrical coordinates, allowing a more detailed and precise representation of its internal structure. Simultaneously, the formation of overly fine grids near the trunk surface is prevented, thereby reducing computational demands and enhancing efficiency. Based on the unique characteristics of the trunk, the Kirchhoff migration approach allows the imaging aperture to be optimized, improving both the accuracy of imaging within the trunk and computational efficiency, while also simplifying operational procedures.

III. Measurement and Signal Processing

A. Dual-polarized GPR System and Survey Strategy

This study leverages the advanced capabilities of the compact dual-polarized "Aladdin" Ground Penetrating Radar (GPR) system, developed by IDS GeoRadar, a division of Hexagon (as illustrated in Fig. 5(a)). The Aladdin GPR system is equipped with two 2 GHz antennas that are polarized perpendicular to each other, operating in HH and VV channels. This dual-polarized configuration enables the simultaneous acquisition of polarimetric data, providing a comprehensive view of subsurface structures [35]. Figure 5(b) depicts the antenna configuration, showcasing the perpendicular alignment

crucial for capturing polarized signals. A unique feature of dual polarization significantly enhances the depth penetration capabilities of the system. By simultaneously acquiring data in both the HH and VV channels, the Aladdin GPR system allows for comprehensive subsurface profiling, offering insights into shallow and deep structures alike. This capability is particularly advantageous for surveying applications requiring a nuanced understanding of subsurface features, making the Aladdin GPR system a valuable tool for this study.

The field inspection measurement is performed on a live tree at Walpole Park, London in the U.K. Considering its bark color and health condition at the time of the inspection, we were able to roughly diagnose that the tree was suffering from disease. The height of the tree was about 15 m, and the radius of the trunk was approximately 40 cm. This study lies in the strategic

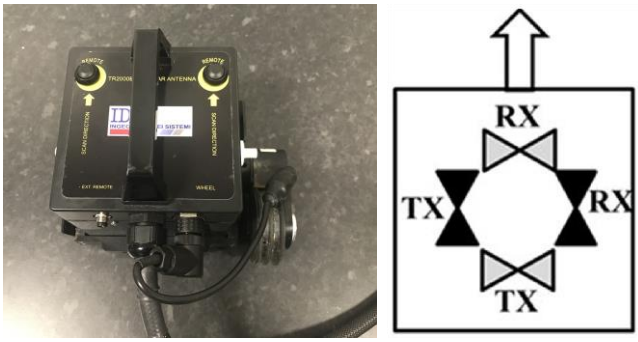

Fig. 5. Dual-polarized "Aladdin" Ground Penetrating Radar system and antenna configuration.

capture of 132 photographs from diverse visual angles and distances using a Canon EOS camera and 18 mm fixed focal length lens. This meticulous photograph dataset encompasses a comprehensive range of perspectives, laying the groundwork for a detailed 3D DEM reconstruction. Fig. 6 serves as a visual testament to the success of the SfM techniques, showcasing a 3D model of the tree trunk derived from four distinct viewpoints. Two white circle strings with 40 cm interval and a central green circle string were designed and set during the GPR survey. This geometric configuration facilitates the calculation of the scale factor $s_{m,n}$ - a crucial parameter in the subsequent analysis.

Having obtained the intricate 3D geometry of the tree trunk, the next step is to extract the cross-sectional outline of the trunk at the precise height of the GPR survey trace. This measurement requires 21 GPR surveys, each conducted at 2 cm intervals between two marked white circles, as shown in Fig. 7. In the figure, blue circles indicate the GPR survey traces, and red stars mark the initiation points for each survey trace. This consistent spacing ensures that GPR measurements are evenly distributed across the cross-section, allowing comprehensive data coverage.

The 3D geometry of the tree trunk, achieved with sub-centimeter precision, offers a level of spatial accuracy much finer than the resolution of the using dual-polarized GPR system. This high level of detail enables each GPR trace to align precisely with the surface structure, significantly enhancing the accuracy of the subsurface imaging process. Such precision is

Fig. 6. 3D model of tree trunk derived from four distinct views.

critical in the context of tree trunk inspection, where it allows for more accurate mapping of internal anomalies, like decay or voids, in direct relation to the surface structure of the tree. The ability to correlate GPR-detected subsurface features with a highly accurate surface model is instrumental for identifying decay-prone areas or other structural issues within the tree that might otherwise be missed. This innovative approach not only improves the precision of GPR-based subsurface analysis but also sets a new standard for studying the spatial intricacies of tree trunks. By integrating high-resolution 3D geometry with GPR data, researchers can gain unprecedented insights into the internal structure of trees.

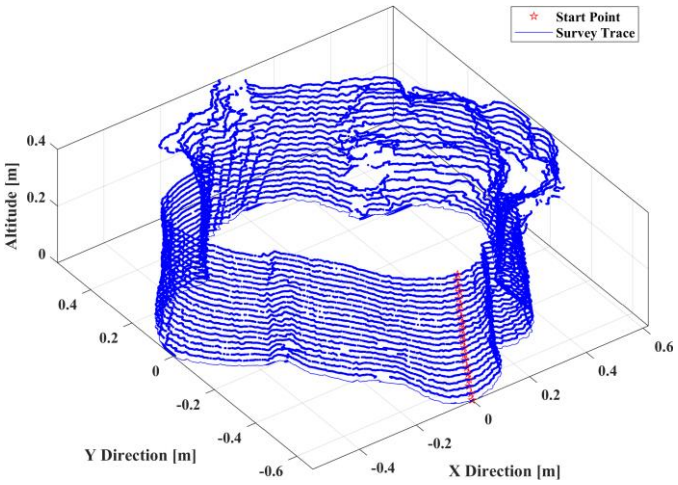

Fig. 7. GPR survey traces extracted from 3D model generated using SfM technique.

B. Data Pre-processing

Before interpreting the raw data, a pre-processing step was implemented to reduce unwanted reflections and improve the SNR. This involved three key procedures. First, time-zero adjustment was applied, ensuring proper alignment of GPR signals by marking the moment the radar signal leaves the antenna. This alignment is essential for accurate data processing. Second, antenna coupling removal was performed to eliminate interference between the transmitter and receiver, which can cause noise and obscure important reflections. Third, background removal techniques, including subtracting the background signal, enhanced the clarity of source signals. Finally, band-pass filtering was used to remove noise while preserving critical signal information. A filter with frequencies between 1.2 GHz and 2.8 GHz was applied, improving data quality and revealing hidden patterns. These pre-processing steps significantly enhanced the clarity and reliability of the data, enabling more accurate analysis and interpretation of GPR signals.

C. Holographic Radar Tomography

In a thriving tree, moisture distribution within the trunk is uniform, gradually rising from the outer bark to the inner core. The moisture content of living trees typically ranges from 35% to 60% [36]. Any disruption, such as decay or a hollow in the center of trunk, significantly alters its dielectric constant, signifying a fundamental shift in the integrity of wood at the boundary of healthy tissue. The moisture gradient is essential for the health and structural stability of the tree to be sustained. An even distribution of water throughout the trunk ensures proper nutrient transport and structural support, preventing weaknesses that could compromise the vitality of trees. Consequently, any deviation from this balanced moisture level, such as decay or damage, is understood to have profound effects on the health and longevity of the tree. By monitoring changes in moisture content and dielectric properties, arborists and researchers can gain insights into the internal health and structural integrity of trees, aiding in their preservation and management.

Using the proposed holographic radar tomography processing procedures described by Eq. (12), representative results are shown in Fig. 8. In these profiles, clear reflections can be observed even within the deep regions - up to 15 ns. Compared to the pro-processing data (HH and VV profiles shown in Fig.8), the SNR of the reconstructed waveform has greatly improved. This depth is much deeper than the conventional observation of a real trunk using GPR. Conventionally, the fusion HH and VV profile method replies on cross correlation, which is a mathematical processing approach [19]. The application conditions for traditional methods are relatively stringent, limiting their suitability for a wide range of measurement scenarios. Moreover, these methods often lack a clear physical foundation making the interpretation of the results more difficult. For instance, regions with high values in traditional correlation analyses may indicate areas of high correlation but do not necessarily correspond to areas with significant changes in relative permittivity ε_r. This ambiguity reduces the reliability and clarity of such methods. In contrast, the processing method proposed in this paper addresses these limitations by offering clear physical significance. It not only accurately identifies regions with considerable changes in ε_r but also significantly improves the SNR, ensuring more reliable and interpretable results.

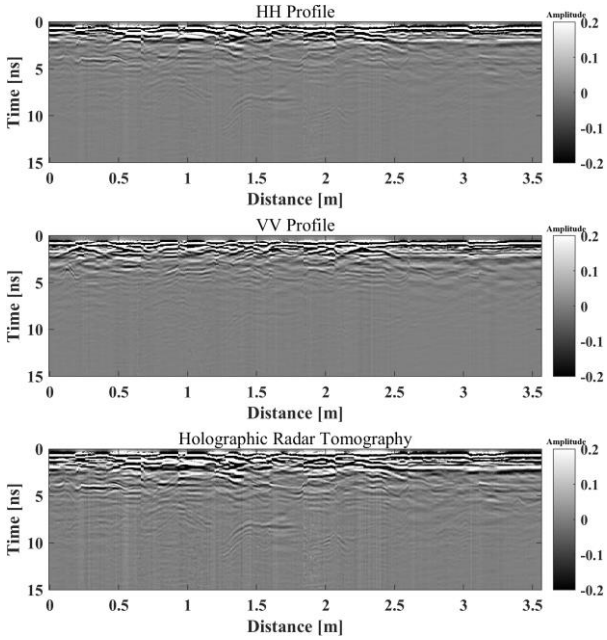

Fig. 8. B-scans of tree trunk before and after holographic radar tomography processing.

D. Kirchhoff Migration

The arc-shape Kirchhoff migration approach is a variation of this method that aims to improve the accuracy and resolution of images, particularly in areas with complex features. By incorporating curved survey paths, the arc-shape Kirchhoff migration approach can produce more accurate images of trunk structures, especially in regions where traditional migration methods may struggle to provide clear imaging. This technique is particularly useful in tree trunk inspection, where accurately imaging inner structures is crucial for identifying critical features on diseased trees.

According to the moisture content of the tree trunk and weather condition, relative permittivity ε_r is given as 20 to reconstruct the 3D images when applying the proposed arc-shaped Kirchhoff migration algorithm. Based on the experience of authors, the relative permittivity of tree trunks in the UK typically ranges between 25 and 30. In winter, due to abundant rainfall, relative permittivity is closer to 30, while in summer, it tends to be closer to 25. However, given the timing of this measurement, the UK had just experienced an extreme drought with high temperatures, and the measurement was conducted on an exceptionally hot day. Therefore, selecting a relative permittivity of 20 is more in line with the actual conditions. Due to the antenna radiation pattern and shape of the tree trunk, 90° is selected as the imaging aperture α of Eq. (13). The following imaging resolutions are selected to reconstruct the 3D images: azimuth angle 1°, radial resolution 0.25 cm and vertical resolution 1 cm. The reconstructed 3D images are presented and discussed in the next section.

IV. Results and Discussions

The findings depicted in Fig. 9 offer a comprehensive view of the reconstructed segments spanning from the base to the apex of the examined tree trunk. Through meticulous examination, distinct patterns emerge, shedding light on the internal dynamics of the trunk. One of the most conspicuous features revealed by the reconstruction is the presence of high-energy areas, which are identified as indicators of anomalies located within the interior of the trunk. These anomalies, intriguingly, tend to cluster in the regions proximal to the bark, hinting at a potential correlation between the structural integrity of the trunk and its external environment. Delving deeper into the analysis, a particularly noteworthy discovery surfaces within the midsection of the trunk, spanning from approximately 15 cm to 23 cm from the base. Here, sub high-energy areas manifest in select regions, introducing a nuanced dimension to the investigation. These localized fluctuations in energy levels suggest subtle deviations in relative permittivity compared to the surrounding regions. Such deviations, while seemingly minor, are considered to hold significant implications, as they point to underlying processes that may be influencing the overall health and stability of the trunk.

Decay, as a natural phenomenon intrinsic to aging trees, can manifest in various forms, ranging from fungal infestations to structural weaknesses. The identification of energy anomalies of reconstructed images is regarded as a vital diagnostic tool, providing insights into the evolving dynamics of the internal composition of the trunk. Equally noteworthy is the absence of closed anomaly areas across all sections of the reconstruction images. This observation carries profound implications, as it effectively rules out the presence of hollow spaces within the surveyed tree trunk. Hollow spaces – often indicative of severe structural compromise – pose a significant threat to the overall stability and longevity of a tree. By confirming the absence of such anomalies, reconstruction images of the structural integrity, providing reassurance regarding its capacity to withstand external stresses and environmental pressures.

Figures 10(a), 11(a), 12(a) and 13(a) present perspective views showcasing the resultant high-energy areas in three dimensions of the trunk under investigation. Correspondingly, the actual photographs of the tree are depicted in Figs. 10(b), 11(b), 12(b) and 13(b), respectively. A detailed examination of these visual representations offers valuable insights into the health and structural integrity of the tree. Beginning with Fig. 10(a), a prominent feature is discernible extending from the base of the trunk and spanning approximately the entire height of the investigated volume – black ellipse area. Remarkably, this feature closely corresponds to the area of bark color anomaly depicted in Fig. 10(b) - black ellipse area. The alignment between the high-energy area observed in the 3D rendering and the actual anomaly captured in the photograph lends credence to the accuracy of the reconstruction process. In Fig. 11(a), however, the high-energy features are notably absent from the side view presented. This absence suggests that the trees observed from this vantage point are in healthy condition. This observation is further corroborated by the uniformity of bark color observed in Fig. 11(b), reaffirming the robust health on this side.

Moving on to Fig. 12(a), a distinct feature is evident at the bottom of the 3D representation – black circle area, corresponding precisely with the damaged segment depicted black circle area in Fig. 12(b). The concordance between the visual evidence in both the reconstructed image and the photograph underscores the efficacy of the imaging technique in accurately identifying structural anomalies within the trunk. Finally, in Fig. 13(a), a significant feature extending throughout the trunk on this side is prominently visible in the upper portion of the image - black ellipse and rectangular region. Upon closer inspection, it becomes apparent that this feature aligns seamlessly with the dark bark region depicted with a black ellipse and rectangular region in Fig. 13(b). This correspondence further strengthens the association between high-energy areas identified through imaging and observable anomalies within the tree. Based on the comprehensive analysis of the results presented, several key conclusions can be drawn regarding the health and integrity of the tree under investigation. Firstly, the presence of a fungal infection extending from the bark to the interior is evident, as evidenced by the alignment between high-energy areas and observable anomalies in the structure of the tree trunk. Secondly, the absence of internal hollows within the tree suggests that its overall structural integrity remains relatively intact. It is crucial to note that, while the structural integrity of the tree is not

significantly compromised, the presence of the fungal infection requires ongoing monitoring to assess its progression and potential impact on the health of the tree.

V. Conclusion

In this study, a set of signal processing methodologies was developed to assess trunk health using GPR, with the primary goal of detecting early signs of decay and small cavities in order to allow for timely intervention and treatment. Such early detection aims to prevent the need for later pruning or tree removal. However, the application of traditional GPR signal processing techniques to living trees presents several challenges, owing to their complex structure, electromagnetic properties, and irregular shapes. To address these challenges, a

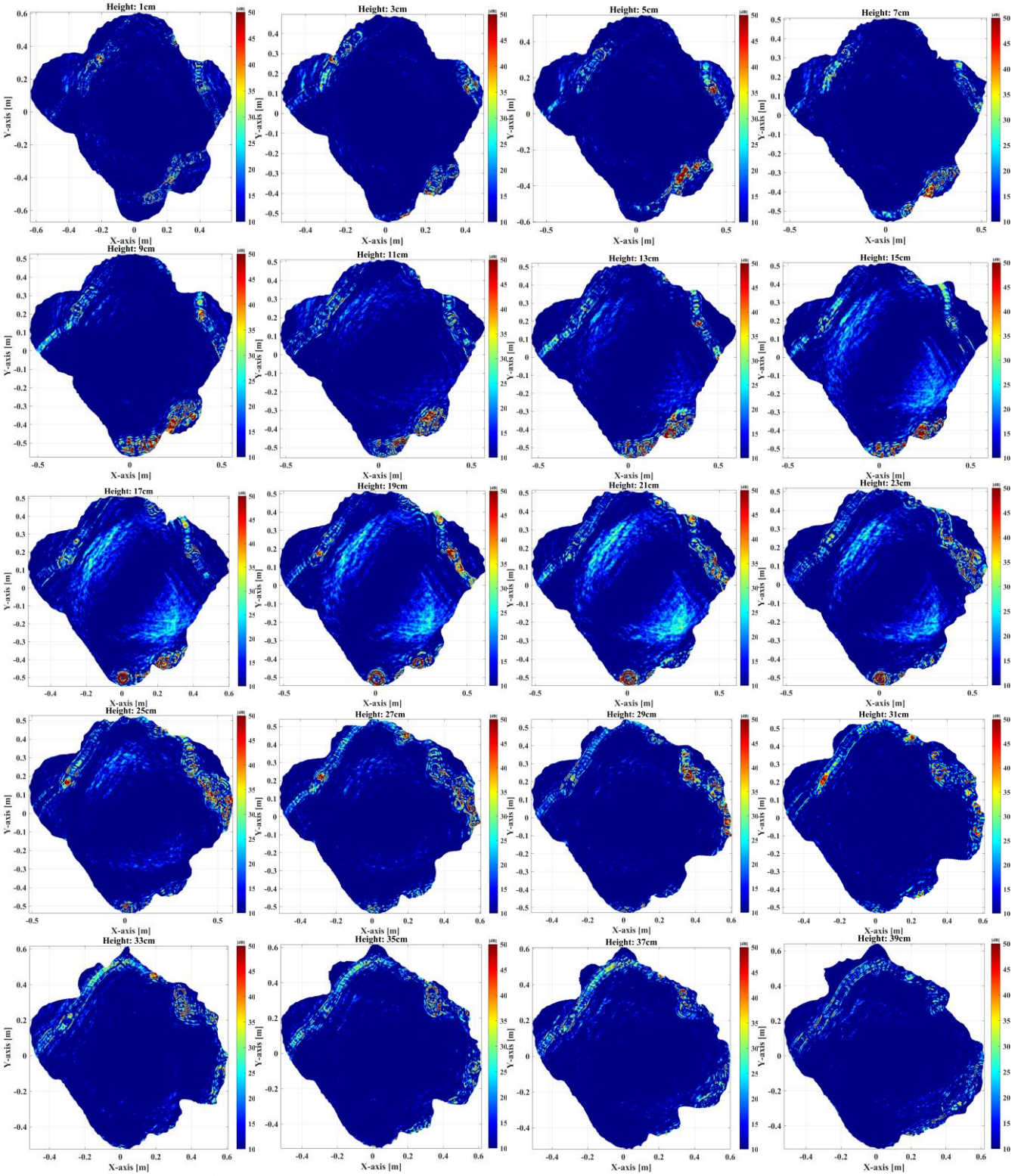

Fig. 9. Reconstruction images of investigated tree trunk sections.

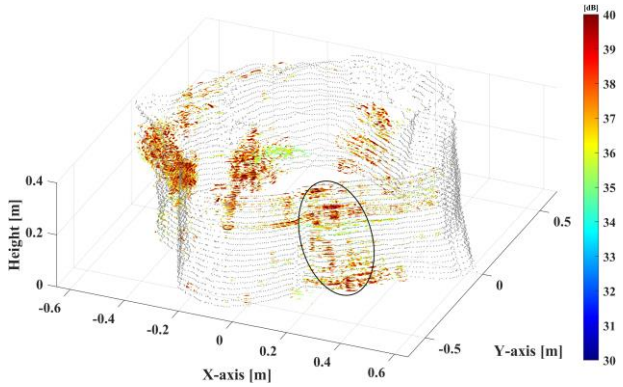

(a)

(b)

Fig. 10. Reconstruction 3D images and real photograph of investigated tree trunk.

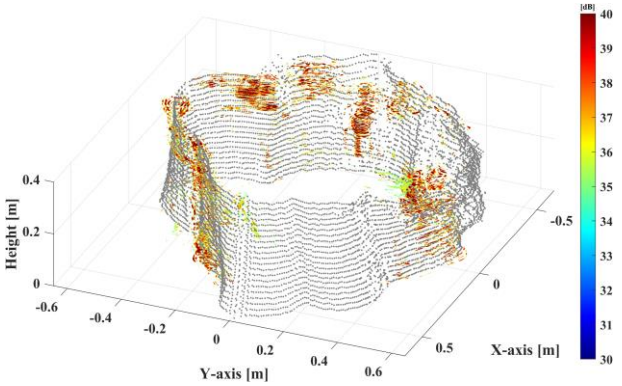

(a)

(b)

Fig. 11. Reconstruction 3D images and real photograph of investigated tree trunk.

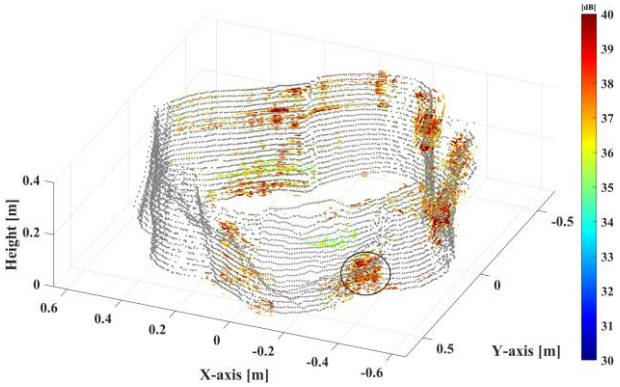

(a)

(b)

Fig. 12. Reconstruction 3D images and real photograph of investigated tree trunk.

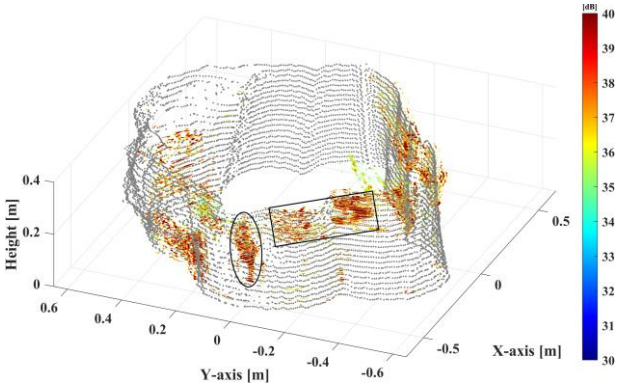

(a)

(b)

Fig. 13. Reconstruction 3D images and real photograph of investigated tree trunk.

novel approach was proposed, integrating SfM photogrammetry, holographic radar tomography, and arc-

shaped Kirchhoff migration. This comprehensive methodology was designed to improve the efficiency and effectiveness of tree disease monitoring.

Initially, SfM was incorporated during GPR surveys to enable the accurate reconstruction of the 3D shape of the tree trunk. By using SfM technology, the 3D positioning of the GPR operating track could be precisely interpolated, enhancing the spatial accuracy of data collection. Following this, a novel holographic radar tomography procedure was developed, which combined HH and VV polarization reflections to transform GPR reflections into relative permittivity multiplied by a scaling factor, significantly improving the SNR. Finally, the arc-shaped Kirchhoff migration algorithm was employed to mitigate the effects of the irregular shape of the trunk, further refining the accuracy of subsurface imaging.

The proposed data processing framework was successfully validated through measurements on real tree trunks, demonstrating the seamless integration of these advanced methodologies. This integrated approach not only provides a detailed and precise representation of both the external and internal features of tree trunks but also establishes a robust framework for merging visual and radar data. However, the innovative technology used in this study is demanding in terms of measurement conditions. It requires sufficient light and a uniform surface texture of the tree trunk. It also requires a lot of preparation, measurement and calculation time.

REFERENCES

[1] G.M. Woodwell and O. Ullsten, *Forests in a full world*. Yale University Press, 2001.

[2] W. Ciesla, *Forest entomology: a global perspective*. John Wiley & Sons, 2011.

[3] D. D. Chiras, *Environmental Science*. Jones & Bartlett Publishers, 2009.

[4] D.B. Lindenmayer and W.F. Laurance, "The ecology, distribution, conservation and management of large old trees," *Biol. Rev.*, vol. 92, no. 3, pp. 1434-1458, Aug. 2017.

[5] M. Kõrkjas, L. Remm, A. Lõhmus, "Development rates and persistence of the microhabitats initiated by disease and injuries in live trees: A review," *For. Ecol. Manag.*, vol. 482, pp. 118833, Feb. 2021.

[6] A. M. Alani et al. "Reverse-time migration for evaluating the internal structure of tree-trunks using ground-penetrating radar," *NDT&E Int.*, vol. 115, pp. 102294, Oct. 2020.

[7] P. Palma and R. Steiger, "Structural health monitoring of timber structures–Review of available methods and case studies," *Constr. Build. Mater.*, vol. 248, no. 118528, Jul. 2020.

[8] I. Giannakis et al. "Health monitoring of tree trunks using ground penetrating radar," *IEEE Trans. Geosci. Remote Sens.*, vol. 57, no. 10, pp. 8317-8326, Jun. 2019.

[9] I. Giannakis et al. "Diagnosing emerging infectious diseases of trees using ground penetrating radar," *IEEE Trans. Geosci. Remote Sens.*, vol. 58, no. 2, pp. 1146-1155, Oct. 2019.

[10] L. Liu and G. Li, "Acoustic tomography based on hybrid wave propagation model for tree decay detection," *Comput. Electron. Agric.*, vol. 151 pp. 276-285, Aug. 2018.

[11] A. Galieni et al. "Past and future of plant stress detection: an overview from remote sensing to positron emission tomography," *Front. Plant Sci.*, vol.11, pp. 609155, Jan. 2021.

[12] J. Wicke, G.A. Dumas and P.A. Costigan, "Trunk density profile estimates from dual X-ray absorptiometry," *J. Biomech.*, vol. 41, no. 4, pp. 861-867, Jan. 2008.

[13] A. Arciniegas, L. Brancheriau and P. Lasaygues, "Tomography in standing trees: revisiting the determination of acoustic wave velocity," *Ann. For. Sci.*, vol. 72, pp. 685-691, Sep. 2015.

[14] Q. Qiu et al. "An innovative tomographic technique integrated with acoustic-laser approach for detecting defects in tree trunk," *Comput. Electron. Agric.*, vol. 156, pp. 129-137, Jan. 2019.

[15] L. Espinosa et al. "Effect of wood anisotropy in ultrasonic wave propagation: A ray-tracing approach," *Ultrason.*, vol. 91, pp. 242-251, Jan. 2019.

[16] J. Hruska, J. Čermák and S. Šustek, "Mapping tree root systems with ground-penetrating radar," *Tree Physiol.*, vol. 19, no. 2, pp. 125-130, Feb. 1999.

[17] A. Aboudourib, M. Serhir and D. Lesselier, "A processing framework for tree-root reconstruction using ground-penetrating radar under heterogeneous soil conditions," *IEEE Trans. Geosci. Remote Sens.*, vol. 59, no. 1, pp. 208-219, May 2020.

[18] W. Luo et al. "Accurate tree roots positioning and sizing over undulated ground surfaces by common offset GPR measurements," *IEEE Trans. Instrum. Meas.*, vol. 71, pp. 1-11, Jun. 2022.

[19] L. Zou and F. Tosti and A.M. Alani. "Nondestructive inspection of tree trunks using a dual-polarized ground-penetrating radar system," *IEEE Trans. Geosci. Remote Sens.*, vol. 60, pp. 1-8, Jun. 2022.

[20] D. Feng et al. "Inspection and imaging of tree trunk defects using GPR multifrequency full-waveform dual-parameter inversion," *IEEE Trans. Geosci. Remote Sens.*, vol. 61, pp. 1-15, Feb. 2023.

[21] Z. Chen et al. "Internal decay inspection of tree trunks using 3D point cloud and reverse time migration of ground penetrating radar data," *NDT & E Int.*, vol. 137, pp. 102853, Jul. 2023.

[22] H. He et al. "Time and frequency domain reflectometry for the measurement of tree stem water content: A review, evaluation, and future perspectives," *Agric. For. Meteorol.*, vol. 306, pp. 108442, Aug. 2021.

[23] L. Zou et al. "Surface Permittivity Estimation of Southern Utopia Planitia by High-Frequency RoPeR in Tianwen-1 Mars Exploration," *IEEE Trans. Geosci. Remote Sens.*, vol. 62, pp. 1–9, 2024, Art. no. 2002809.

[24] R. Jing et al. "Above-bottom biomass retrieval of aquatic plants with regression models and SfM data acquired by a UAV platform–A case study in Wild Duck Lake Wetland, Beijing, China," *ISPRS J. Photogramm. Remote Sens.*, vol. 134, pp. 122-134, Dec. 2017.

[25] D. Feurer and F. Vinatier, "Joining multi-epoch archival aerial images in a single SfM block allows 3-D change detection with almost exclusively image information," *ISPRS J. Photogramm. Remote Sens.*, vol. 146, pp. 495-506, Dec. 2018.

[26] S. Jiang, C. Jiang and W. Jiang, "Efficient structure from motion for large-scale UAV images: A review and a comparison of SfM tools," *ISPRS J. Photogramm. Remote Sens.*, vol. 167, pp. 230-251, Sep. 2020.

[27] R. Szeliski, *Computer Vision: Algorithms and Applications*, Berlin, Germany: Springer, 2010.

[28] F. Santoso, M. A. Garratt and S. G. Anavatti, "Visual–inertial navigation systems for aerial robotics: Sensor fusion and technology", *IEEE Trans. Autom. Sci. Eng.*, vol. 14, no. 1, pp. 260-275, Jan. 2017.

[29] M.R. James and S. Robson, "Straightforward reconstruction of 3D surfaces and topography with a camera: Accuracy and geoscience application," *J. Geophys. Res. Earth Surf.* vol. 117, no. F03107, pp. 1-17, Sep. 2012.

[30] S. Lambot and F. André, "Full-wave modeling of near-field radar data for planar layered media reconstruction," *IEEE Trans. Geosci. Remote Sens.*, vol. 52, no. 5, pp. 2295-2303, May 2013.

[31] A. De Coster and S. Lambot, "Full-wave removal of internal antenna effects and antenna–medium interactions for improved ground-penetrating radar imaging," *IEEE Trans. Geosci. Remote Sens.*, vol. 57, no. 1, pp. 93-103, Jul. 2018.

[32] P.H. Pathak and R.J. Burkholder, *Electromagnetic radiation, scattering, and diffraction*. John Wiley & Sons, 2021.

[33] X. Feng and M. Sato, "Pre-stack migration applied to GPR for landmine detection," *Inverse Probl.*, vol. 20, no. 6, pp. S99, Nov. 2004.

[34] X. Feng, M. Sato and C. Liu, "Hand-held GPR imaging using migration for irregular data," *IEEE J. Sel. Top. Appl. Earth Obs. Remote Sens.*, vol. 4, no. 4, pp. 799-803, Sep. 2011.

[35] J. Lachowicz and M. Rucka, "A novel heterogeneous model of concrete for numerical modelling of ground penetrating radar," *Constr. Build. Mater.*, vol. 227, pp. 116703, Dec. 2019.

[36] C. Skaar, *Wood-water relations*. Springer Science & Business Media, 2012.